Bayesian approach to background subtraction for data from the extended x-ray-absorption fine structure

H. J. Krappe and H. H. Rossner
Hahn-Meitner-Institut Berlin, Glienicker Strasse 100, D-14091 Berlin, Germany
(Received 27 January 2004; published 3 September 2004)

We construct the x-ray-absorption fine structure (XAFS) function $\chi(k)$ from measured absorption data $\mu(E)$, using a Bayesian approach. In particular, an empirical correction to the embedded-atom absorption coefficient μ_0—as obtained by the code FEFF—and the energy-dependent overall efficiency of the experimental setup is determined. This procedure is combined with a Bayesian analysis of the χ function in terms of structural parameters, reported earlier, to a uniform method of XAFS data evaluation. The method can be generalized to the case of overlapping *L*-edge data and yields simultaneously the background-subtraction parameters for the three *L*-edge contributions, besides the structural parameters of the lattice. We apply the method to XAFS data measured on germanium and computer-generated *L*-edge iron data.

DOI: 10.1103/PhysRevB.70.104102 PACS number(s): 61.10.Ht, 07.05.Tp, 87.64.Fb

I. INTRODUCTION

In order to extract the x-ray-absorption fine structure (XAFS) expression $\chi(k)=\mu(k)/\mu_0(k)-1$ as a function of the photoelectron wave number k from absorption data $\mu_{\rm exp}(E)$, measured at energies E, estimates are needed for (i) the background absorption $\mu_{\rm back}(E)$, not originating from the reaction one wants to analyze, (ii) the overall efficiency $A(E)$ of the experimental setup, and (iii) various many-electron corrections[1,2] to the embedded-atom absorption coefficient $\mu_0^{(1)}(k)$ and the XAFS function $\chi^{(1)}(k)$. This function is obtained from *ab initio* XAFS codes like FEFF[3] in terms of the distances R_i of the first I shells surrounding the absorbing atom and the projected Debye-Waller (DW) parameters σ_j^2 of the J different scattering paths of the photo electron within the cluster of these shells.

In the following we will quantify the uncertainties connected with the input data and with the models available for the fit, and discuss the resulting uncertainties of the fitted geometrical parameters. In particular, we will parametrize some of the uncertainties of the normalization and of the model in terms of a few empirical parameters, which are to be determined by the fit. These auxillary model parameters are finally integrated out of the joint *a posteriori* probability distribution for the model parameters.

II. ANSATZ FOR THE FIT OF *K*-EDGE XAFS DATA

We assume that the smooth part $\overline{\mu}_{\rm back}$ of the background can be obtained by standard polynomial extrapolation from the preedge to the postedge region.[4] We then apply the smoothing procedure described in the appendix to the difference $\mu_{\rm exp}-\overline{\mu}_{\rm back}$ and obtain $\overline{\mu}_{\rm exp}$. The smoothing removes the oscillatory XAFS stucture without affecting the steep rise at the threshold $E_0^{\rm (prior)}$. The same smoothing procedure is applied to the embedded-atom absorption coefficient $\mu_0^{(1)}$ obtained from FEFF8. This time, oscillations due to resonances of the photoelectron in its muffin-tin potential well are removed. Then, with $k^2=2m\hbar^{-2}[E-E_0^{\rm (prior)}]$, the appropriate normalization factor of the data to the embedded-atom strength $\mu_0^{(1)}$ is $A(k)=\overline{\mu}_{\rm exp}(k)/\overline{\mu}_0^{(1)}(k)$. This quantity can be interpreted as the overall efficiency of the experimental setup. We assumed that $A(k)$ is a smooth function. If, however, the beam intensity oscillates as a function of the energy, our ansatz for $A(k)$ cannot be used. Additional information on the variation of the beam intensity with energy is needed in this case.

Our determination of the normalization function $A(k)$ is very similar to the procedure proposed by Bulgaev *et al.*[5] However, we do not use a folding procedure for smoothing because of the dangerously long range of edge effects connected with folding, in particular at the absorption edge.

For a variety of reasons the FEFF result for μ_0 needs corrections. Discontinuities in the derivatives of the muffin-tin approximation of the potential lead to spurious reflections and a corresponding peak in the *r*-space transform of the XAFS function around $R_1/2$.[1] In addition, many-electron effects tend to dampen and shift the resonance structure.[1] The factorization approximation in Eq. (44) of Ref. 2 neglects this effect. To account for all these corrections we write $\mu_0(k)=\mu_0^{(1)}(k)+\delta\mu_0(k)$, where $\delta\mu_0(k)$ will be represented by a cubic spline on an equally spaced grid of support points, whose number T is to be chosen to make the spline just sufficiently flexible for the purpose for which it is introduced. The ordinates $\delta\mu_t$, $t=1,\ldots,T$ are treated as model parameters to be determined together with all other model parameters in the fit. A similar correction to $\mu_0^{(1)}$ was proposed by Klementev.[6]

The task is, therefore, to fit

$$\mu_{\rm exp}(k)-\overline{\mu}_{\rm back}(k)=A(k)[\mu_0^{(1)}(k)+\delta\mu_0(k;\delta\mu_1,\ldots,\delta\mu_T)]\times[\chi(k)+1], \quad (1)$$

where χ is given in the extended x-ray-absorption fine-structure (EXAFS) energy range for monoatomic, unoriented samples by the multiple-scattering sum[7,8]

$$\chi(k) = \frac{S_0^2}{k}\sum_j N_j \frac{|f_j(k,R_j)|}{R_j^2} e^{-2k^2\sigma_j^2 - 2R_j/\lambda(k)} \times \sin\left[2k(R_j - \delta R_j) + \phi_j(k) - \frac{4}{3}C_{3,j}k^3\right], \quad (2)$$

with the wave number k and length corrections $\delta R_j = 2\sigma_j^2(R_j^{-1}+\lambda^{-1})$, in terms of the model parameters R_j, $j = 1,\ldots,J$, the half-path distances of the J scattering paths considered in the multiple-scattering sum, N_j, σ_j^2, and $C_{3;j}$, the multiplicities of equivalent scattering paths, the DW parameters, and the anharmonicity parameters, respectively, and finally the effective edge energy E_0, which determines k.

In view of the results of Ref. 2 one expects each term in the sum (2) to be multiplied by a complex amplitude $S_j^2(k)$ because of the many-electron effects. These quantities seem to be rather independent of the wave number k, at least in the range of the extended x-ray absorption fine structure. FEFF yields $S_j^2(k)$ as the product $S_0^2 a_{\rm red}(k)$, real. We therefore define $\overline{|S_j^2|}$ as the average of $|S_j^2(k)|$ over k, $k \geqslant 2.8$ Å^{-1}, and absorb the remaining k dependence in the uncertainties of the products $a_{\rm red}(k)f_j(k)$. The conventional factor S_0^2 in Eq. (2) is identified with the average of $\overline{|S_j^2|}$ over the index j. We will treat the factor S_0^2 as a model parameter to be determined in the fit. The deviations of $\overline{|S_j^2|}$ from S_0^2 may be absorbed in the N_j, whereas the phase of $S_j^2(k)$ can be absorbed in the scattering phase $\phi_j(k)$. The form of Eq. (1) implies that the wiggly part of the background absorption $\mu_{\rm back} - \overline{\mu}_{\rm back}$—if there is any—is absorbed in $\delta\mu_0(k)$.

III. STOCHASTIC REGULARIZATION

To treat high-dimensional, ill-posed fit problems, we used in Ref. 9 the concept of an *a priori* guess of the set of model parameters and reformulated the fitting task by looking for the shift of the model parameters with respect to their *a priori* values, as required by the data. Invoking the maximum-entropy principle, the ill-posed inversion problem can then be regularized.[10] To define the procedure completely one still has to fix the variance matrix $\mathbf{A}$ of the *a priori* model parameters, which determines in particular the weight with which the *a priori* information influences the fit relative to the weight of the experimental data. In Ref. 9 we showed that an optimization condition, first proposed by Turchin and Nozik[11] to obtain an overall weight parameter for the *a priori* input data, admits a generalization such that the relative weights for several groups of *a priori* model parameters, in particular those of different dimensions, can be determined independently. They follow from Eq. (34) of Ref. 9 and must not be assumed ad hoc. This is a decisive improvement of our approach compared to many other applications of Bayesian methods in data analyses.

It is easy to extend the implementation of this scheme, presented in Ref. 9, to include the determination of the additional model parameters $\delta\mu_t$. Instead of using $\chi(k_l)$, $l = 1,\ldots,L$, as input, we now take $\mu_{\rm exp}(k_l)$ with Eqs. (1) and (2) and add the $\delta\mu_t$ to the components of the vector of model parameters $\mathbf{x}$. It is important to remember that the stochastic regularization method does not require an *a priori* restriction of the number of model parameters. Instead, it automatically determines that subspace $\mathcal{R}$ of the whole model-parameter space $\mathcal{Q}$, where the data determine the outcome of the fit. In the complementary subspace the result is determined by the values $x_n^{(0)}$ given *a priori* to the model parameters. Strong error correlations between two model parameters indicate that the data do not determine them independently.

The result of the fit consists of an N-dimensional Gaussian *a posteriori* probability over the N-dimensional space $\mathcal{Q}$. The variance matrix of this distribution is given by $(\mathbf{Q}+\mathbf{A})^{-1}$, where $\mathbf{Q}$ is the information marix.[9] The model parameters S_0^2, E_0, and $\delta\mu_1,\ldots,\delta\mu_T$, are introduced for the sole purpose of accounting for certain systematic deficiencies of the theoretical model underlying the data analysis. Unlike the radii R_i or the DW parameters σ_j^2, they are not of interest themselves. Therefore, we integrate them out of the joint probability in the end.

IV. ANALYSIS OF GERMANIUM DATA

As an example of the procedure proposed above we will analyze the high-quality data obtained by Newville[12] on germanium at 300 K. As in Ref. 9 we retain, in the sum of Eq. (2), the first 20 scattering paths with the largest amplitudes, of which seven are single-scattering paths. The half-lengths R_j of the multiple-scattering paths are expressed by the R_i of the single-scattering paths, assuming a diamond structure. We will further assume that the parameters N_j have their ideal lattice values and will not include them in the set of model parameters to be fitted. The DW parameters σ_j^2 of all 20 scattering paths and the seven anharmonicity parameters $C_{3;i}$ of the single-scattering paths will be treated as independent model parameters.

The input parameters are those given in Table I of Ref. 9. In the smoothing procedures for $\mu_{\rm exp}$ and μ_0, we used the polynomial order $K=5$ and weight parameter $\alpha=1.2$ for $\mu_{\rm exp}$ and $K=7$, $\alpha=0.15$ for μ_0. The number T of support points was chosen to be 21, so that the dimension of the model-parameter space becomes $N=57$. A larger number of support points in the spline leads to increasing error correlations between these parameters without changing the average values of the remaining parameters. The *a priori* values for the $\delta\mu_t$ were all chosen to be zero. It is convenient to take 0.001 of the size of the edge of $\mu_0^{(1)}(k)$ at E_0 as the initial internal scaling $\hat{x}_n$ for $n=1,\ldots,T$. The order of the model parameters in the vector $\mathbf{x}$ is $\delta\mu_1,\ldots,\delta\mu_{21}$, S_0^2, E_0, $R_1,\ldots,R_7$, $\sigma_1^2,\ldots,\sigma_{20}^2$, $C_{3;1},\ldots,C_{3;7}$, and for these six groups of model parameters, the relative widths of their *a priori* probability distributions have been determined independently.

The normalization function $A(k)$ is plotted in Fig. 1. As one expects, $A(k)$ is a smooth function of k. In the lower frame of Fig. 1, the normalized experimental absorption cross-section $\mu_{\rm exp}^{\rm (red)} = [\mu_{\rm exp}(k) - \overline{\mu}_{\rm back}(k)]/A(k)$ is plotted, together with the absorption coefficient $\mu^{\rm (post)}(k)$, resulting from the fit. In addition, we show the embedded-atom absorption coefficients $\mu_0^{(1)}(k)$ and $\mu_0^{\rm (post)}(k)$. Only data with $k \geqslant k_{\rm cut} = 3.3$ Å^{-1} can be used in the fit, since our restriction of

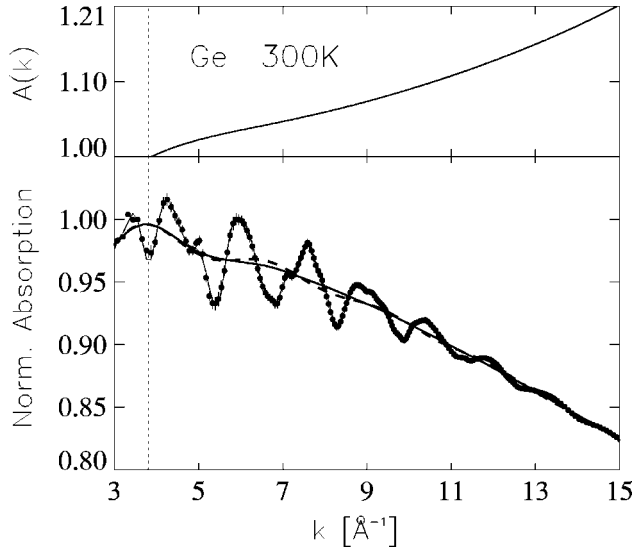

FIG. 1. The efficiency function $A(k)$ for the Ge data of Ref. 12 (upper frame) in units of the edge jump of $\mu_{\rm exp}-\overline{\mu}_{\rm back}$. In the lower frame, data points with errors represent the absorption cross section from Ref. 12 normalized by $A(k)$, $[\mu_{\rm exp}(k)-\mu_{\rm back}(k)]/A(k)$. The thin line gives the result of the fit, $\mu^{\rm post}(k)$, the thick line is $\mu_0^{\rm post}(k)$, the dashed line shows $\mu_0^{(1)}(k)$, the embedded-atom strength from FEFF8. The vertical dotted line is at $k_{\rm cut}$.

the cluster size for the scattering calculation to seven shells and the truncation of the multiple-scattering series (2) make the latter unreliable for smaller k.[9] Actually, we use the somewhat larger $k_{\rm cut}=3.8$ Å^{-1}, indicated by the vertical line in Fig. 1, since $\mu_0^{(1)}(k)$ varies strongly between $k=3.0$ and 3.8 Å^{-1}, which would require smoothing polynomials of rather high order in the construction of $\overline{\mu}_0^{(1)}$. The same experimental and model-related errors were used as in Ref. 9 and are shown there in Fig. 3.

In the upper frame of Fig. 2 we plot the oscillating part of the embedded-atom absorption from FEFF $\Delta\mu_0^{(1)}(k)=\mu_0^{(1)}(k)-\overline{\mu}_0^{(1)}(k)$, which may contain spurious contributions and the corresponding quantity obtained from the fit, $\Delta\mu_0^{(\rm post)}$

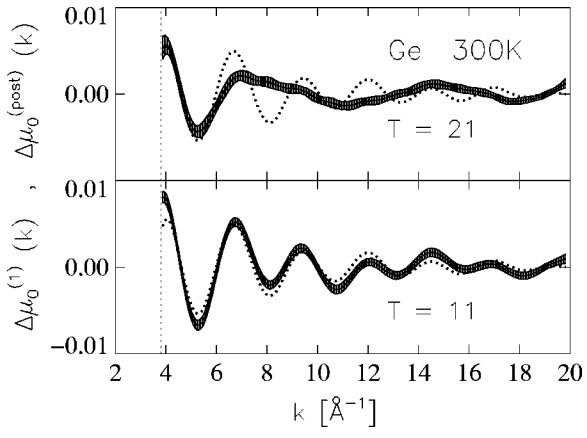

FIG. 2. The dotted line is the oscillating part of the embedded-atom absorption $\Delta\mu_0^{(1)}(k)$, the full line is the oscillating part of the corrected embedded-atom function $\Delta\mu_0^{\rm post}$, together with its error band. Upper frame for $T=21$ spline points, lower frame for $T=11$.

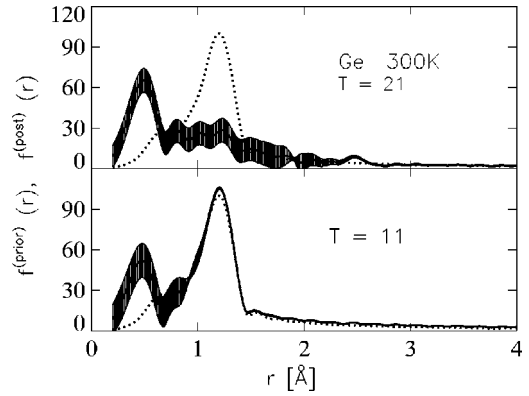

FIG. 3. The functions $f^{(\rm prior)}(r)$ (dotted line) and $f^{(\rm post)}(r)$, together with the error bands (full lines) for $T=21$ in the upper frame, and for $T=11$ in the lower frame.

$=\mu_0^{(\rm post)}-\overline{\mu}_0^{(\rm post)}=\Delta\mu_0^{(1)}+\delta\mu_0-\overline{\delta\mu}_0$. The width of the curve $\Delta\mu_0^{(\rm post)}$ indicates the *a posteriori* one-standard-deviation error. The damping of the oscillations in $\mu_0^{(\rm post)}$ compared to $\mu_0^{(1)}$ is clearly visible. In order to achieve an adequate correction of $\mu_0^{(1)}$, a sufficient number T of spline points is needed. In the lower frame of Fig. 2 we show the function $\Delta\mu_0^{(\rm post)}$ with its error band, calculated for $T=11$. It is seen that an eleven-point spline is too stiff to allow for the required corrections to $\mu_0^{(1)}$.

It is instructive to compare the Fourier transforms of these functions

$$f^{(\rm prior)}(r)=\left|\int_{k_{\rm cut}}^{k_{\rm max}} e^{ikr}\Delta\mu_0^{(1)}(k)dk\right|$$

and

$$f^{(\rm post)}(r)=\left|\int_{k_{\rm cut}}^{k_{\rm max}} e^{ikr}\Delta\mu_0^{(\rm post)}(k)dk\right|.$$

In Fig. 3 the two functions $f^{(\rm prior)}$ and $f^{(\rm post)}$ are plotted together with the *a posteriori* error band, which obtained from

$$[\Delta f(r)]^2=\sum_{t,t'=1}^{T}\frac{\partial f^{(\rm post)}(r;\delta\mu)}{\partial(\delta\mu_t)}(Q+A)^{-1}_{tt'}\frac{\partial f^{(\rm post)}(r;\delta\mu)}{\partial(\delta\mu_{t'})}.$$

Note that the spurious reflection at the edge of the muffin-tin potential, giving rise to the peak of $f^{(\rm prior)}(r)$ at 1.2 Å ($\approx R_1/2$), is no longer present in $f^{(\rm post)}(r)$. The same calculation for $T=11$, plotted in the lower frame, shows again that with an insufficient number of support points, the spurious peak cannot be removed, However, the peak of $f^{(\rm post)}(r)$ around $r=0.5$ Å, accounting for correction to $\mu_0^{(1)}(k)$ from FEFF8 at large k values, shows up in both cases.

The input EXAFS function $\chi(k)=(\mu_{\rm exp}-\overline{\mu}_{\rm back})/[A(k)\mu_0^{(1)}]-1$ is compared in Fig. 4 with the EXAFS function $\chi(k)$, calculated with the corrected μ_0. Also shown is the EXAFS function obtained by the routine AUTOBK (Ref. 13) of the UWXAFS program package[14] using the following parameter settings: k range: [0.05, 19.8] Å^{-1}, k weight: 3, sills window Δk parameters: 0.50 Å^{-1}, 0.50 Å^{-1}, and background

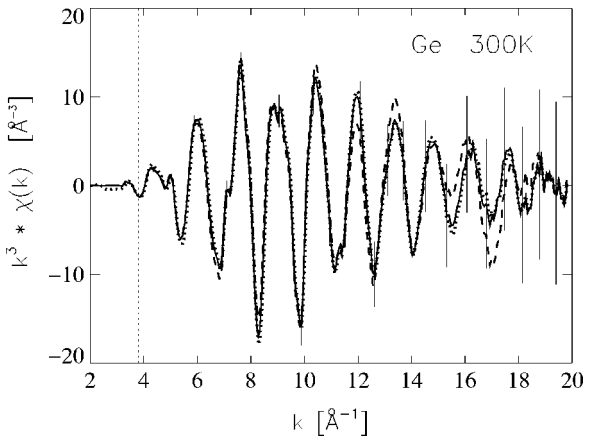

FIG. 4. The EXAFS function $\chi(k)$ in $k^3\chi(k)$ representation. The solid line is the result of our smoothing procedure with the corrected μ_0, the dotted line is calculated with AUTOBK. At some data points, typical error bars are indicated. The dashed line is calculated with the uncorrected μ_0.

r range: $[0.00, 0.98]$ Å. With this choice, the EXAFS functions obtained by AUTOBK and by our smoothing procedure are almost indistinguishable in the relevant *k* range above k_{cut}. The quality of the fit is therefore the same as in Fig. 5 of Ref. 9.

The modulus of the off-diagonal matrix elements of the error-correlation matrix is shown in Fig. 5. There are only small correlations between the $\delta\mu_t$ on the one hand, and the distances R_i and DW parameters σ_j^2 on the other hand, because the correction to μ_0 accounts mainly for effects of the muffin-tin kink in the electron potential around $R_1/2$, which is well separated from the distances R_i of all scattering centers. The function $\mu_0^{(\mathrm{post})}$ is therefore determined fairly unambiguously by the experimental data.

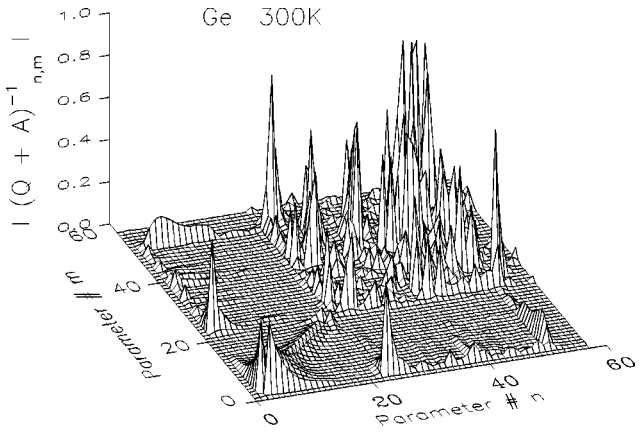

FIG. 5. The modulus of the off-diagonal matrix elements of the *a posteriori* error-correlation matrix. The small peaks at the lower left corner correspond to error correlations between the spline values $\delta\mu_t$ of the first two nodal points. They are also correlated with the parameters S_0 and E_0 (the peak on the lower border at $n=22$ and 23). There are smaller correlations between $\delta\mu_1$ and R_1, at $n=24$ and between the first anharmonicity parameter $C_{3;1}$ and the $\delta\mu_t$ (small ridges at $n=51$. The large peaks around $[m,n]=[25,52]$ refer to correlations between parameters R_i and $C_{3;i}$.

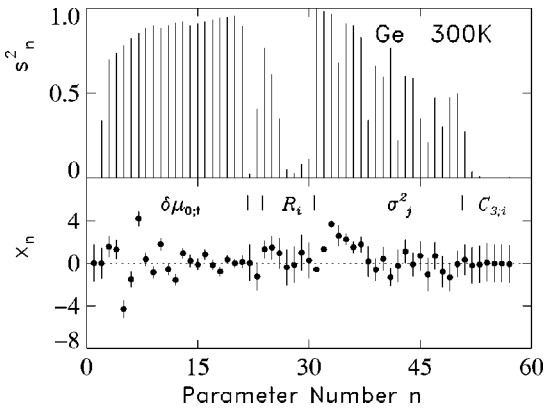

FIG. 6. The deviations of the fitted model parameters from their *a priori* values (lower frame); squared cosines s_n^2 of the projections of the model parameters into the subspace $\mathcal{R}$ of the total model parameter space $\mathcal{Q}$ (upper frame).

In the upper pannel of Fig. 6, the weights s_n^2 are shown, with which the experimental data (rather than the *a priori* information) enter into the fit of the model parameters. As in Ref. 9, $s_n^2=1$ indicates full determination by the data. It is seen that the spline ordinates are well determined—in fact required—by the data. In the lower frame, the deviations of the model parameters from their *a priori* values are plotted together with their *a posteriori* errors in dimensionless units, as in Fig. 6 of Ref. 9. The shifts x_n of the parameters S_0 and E_0 ($n=22$ and 23, respectively) are seen to be compatible with zero. The same holds for all anharmonicity parameters $C_{3;i}$ ($n=51,\ldots,57$) and all radii, except R_1 and R_2, which are shifted upwards by 0.01 Å with an *a posteriori* error of 0.006 Å. Of the DW parameters, the first seven are significantly changed compared to their *a priori* values in a correlated Debye model with a Debye temperature of 360 K. The corresponding data analysis without correction to μ_0, but with the same *a priori* input, was presented in Fig. 6 of Ref. 9. A comparison shows that the trend in the shifts of the DW parameters is the same as before. Also in absolute units, Fig. 7 of Ref. 9, the shifts have the same size in the present calculation. But instead of a minor shift in R_5 obtained in Ref. 9, we now see slight shifts of R_1 and R_2, which is a more plausible result.

V. FIT OF *L*-EDGE DATA

The L_1-, L_2-, and L_3-edge XAFS spectra often overlap in the *k* range of interest. This requires an extension of the background-subtraction procedure presented above. We introduce the shifted wave vectors $k_s^2(k)=k^2-\Delta k_s^2$, $s=1,2,3$, with $\Delta k_s^2=2m\hbar^{-2}[E_0^{(L_s)}-E_0^{(L_3)}]$, and the averaged embedded-atom absorption-coefficients $\overline{\mu_0^{(L_s)}}(k)$ obtained by averaging the FEFF absorption coefficients $\mu_0^{(L_s)}(k_s)$. In FEFF $\mu_0^{(L_s)}[E-E_0^{(L_s)}=50\ \mathrm{eV}]$ is normalized to one for each *s*. Therefore, we need the absolute normalization factors D_s for each of the three cross sections. These quantities are available from FEFF (file "xmu.dat"). We then form the ratios

$$\alpha_s(k) = \frac{D_s \overline{\mu}_0^{(L_s)}(k)}{\sum_{s'=1}^{3} D_{s'} \overline{\mu}_0^{(L_{s'})}(k)}, \quad s = 1,2$$

and the averaged experimental L_3-edge absorption-coefficient $\overline{\mu}_{\rm exp}(k)$ is constructed by averaging $(\mu_{\rm exp} - \overline{\mu}_{\rm back})(1-\alpha_1-\alpha_2)$ with respect to the L_3 edge. The efficiency is then given by $A(k) = \overline{\mu}_{\rm exp}(k)/D_3\overline{\mu}_0^{(L_3)}(k)$.

Instead of the expression (1), we now have to fit

$$\mu_{\rm exp}(k) - \overline{\mu}_{\rm back}(k) = A(k)\sum_{s=1}^{3} D_s[\mu_0^{(L_s)}(k) + \delta\mu_0^{(L_s)}[k;\delta\mu_1^{(L_s)},\ldots,\delta\mu_{T_s}^{(L_s)}]] \times[\chi^{(L_s)}(k)+1] \quad (3)$$

in terms of the model parameters $\delta\mu_t^{(L_s)}$, $s=1,2,3$, $t=1,\ldots,T_s$, $E_0^{(L_s)}$, $S_0^{(s)}$, R_j, σ_j^2, and $C_{3;i}$. In Eq. (3) we add a correction spline to each of the three embedded-atom absorption-coefficients $\mu_0^{(L_s)}$ from FEFF. The three L-edge XAFS functions $\chi^{(L_s)}(k)$ are obtained from FEFF in terms of the model parameters. In order to reduce the number of independent model parameters, we assume that $S_0^{(s)} = S_0$, $s=1,2,3$. The form of Eq. (3) shows that the three $\delta\mu_0^{(L_s)}$ cannot be determined independently. We therefore retain only one correction spline, say $\delta\mu_0^{(L_3)}(k_3) = \delta\mu_0^{(L_2)}(k_2) = \delta\mu_0^{(L_1)}(k_1)$. Finally, we assume that the distances of the L_1 and L_2 edges from the L_3 edge are the ones given by FEFF. Therefore, only one edge energy E_0, that of the L_3 edge, is retained in the fit. The output of the fit consists, besides the efficiency function $A(k)$, of one correction spline $\delta\mu_0$, one energy $E_0 = E_0^{(L_3)}$, one factor S_0, and the structural parameters R_i, σ_j^2, and $C_{3;i}$. All three L-edge components contribute to $\mu_{\rm exp}$, although in practice the L_1 contribution is rather small compared to the other two components.

VI. ANALYSIS OF IRON DATA

In order to test the unfolding of an EXAFS spectrum consisting of three L-edge contributions, we prefer to use computer-generated data. We use FEFF to calculate the six functions $\chi^{(L_s)}(k)$ and $\mu_0^{(L_s)}(k)$, $s=1,2,3$ for iron, where the radii are obtained from the lattice constant $a=2.8665$ Å,[15] assuming an ideal bcc lattice. The DW parameters were generated from a correlated Debye model with a Debye temperature of 420 K. We further assume that $C_{3;i}=0$ and $S_0^2 = 0.986$, as given by FEFF8. Nine shells are taken into account in the FEFF calculations, and altogether $J=61$ paths, corresponding to a 4% amplitude threshold in FEFF. In the k range $[0.05, 20.0]$ Å^{-1}, $L=400$ data points were taken.

Although in a computer simulation the whole energy range from $k=0$ to $k_{\rm max}$ could be used for the fit, we introduce cutoffs for the near-edge XAFS (NEXAFS) ranges of each of the three components of the EXAFS function to simulate the realistic situation, in which the multiple-scattering series (2) cannot be used for small k_s. Since the L_2 and L_3 edges are very close to each other, we introduce one lower cutoff $k_{\rm cut}=3.6$ Å^{-1} to account for the NEXAFS ranges of both the L_2 and L_3 components. Because of the NEXAFS L_1 component, we suppress the k range $[6.0, 6.7]$ Å^{-1}.

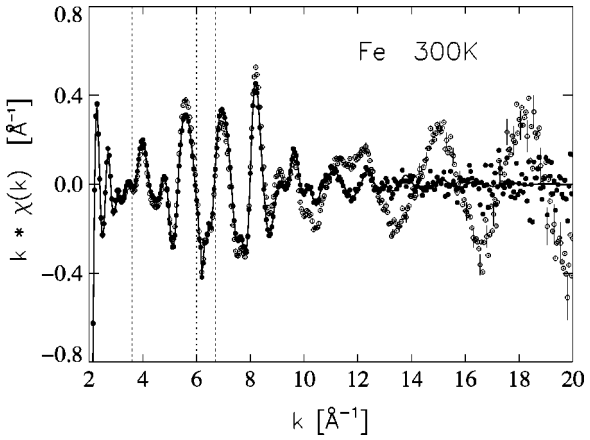

FIG. 7. The full line gives the calculated EXAFS function $\chi(k)$ with $\mu_0^{(L_s)}$ from FEFF8. The open dots are $\chi(k)$ calculated with the distorted $\mu_0^{(L_s)}$ plus statistical errors of the indicated size. The full dots represent the EXAFS function after the distortions $\delta\mu_0^{(L_s)}$ have been corrected out. The k intervals between the left edge of the figure and the first vertical dotted line and between the other two dotted lines are excluded from the fit.

In the computer simulation, the embedded-atom absorption coefficients $\mu_0^{(L_s)}$ are obtained from FEFF8 and are therefore, by construction, the "truth." In order to check whether the fitting procedure can recognize and correct errors in the μ_0's in a realistic fit, we added a distortion to the FEFF result for $\mu_0^{(L_s)}(k_s)$ of the form

$$\delta\mu_0^{(L_s)}(k_s) = 0.01 D_s \sin(2k_s) e^{-0.005k_s^2}, \quad s=1,2,3, \quad (4)$$

with k_s in Å^{-1} in analogy to the germanium case. Of course, this is not meant to imply that in analyzing real XAFS data of iron with FEFF8, corrections to μ_0 of this size are to be expected. The *a priori* values for the $\delta\mu_t$ are chosen to be zero. The *a priori* values of all other model parameters are assumed to be the "true" values, i.e., those used to construct the data. Analogous to the Ge example, the relative weights of the six groups of model parameters have been determined independently.

In Fig. 7, the EXAFS function $\chi(k)$, calculated with the modified $\mu_0(k)$, is compared with the one obtained with the corrected μ_0. Also indicated are the assumed "experimental" errors. The number of spline points was $T=24$ in this calculation. The distortion, Eq. (4), has a drastic effect on the EXAFS function. It is shown in Fig. 8, together with the result of the fit and its error band. A perfect correction of the distortion by the fit would result in a curve compatible with zero within the error band. With $T=24$ spline points, this is still not quite achieved for the smaller k values. But for the choice $T=15$, the situation is considerably worse. This is even more obvious when the Fourier transforms $f^{(\rm post)}(r)$ in Fig. 9 are compared.

In Fig. 10 the shifts of all model parameters, including radii, DW, and asymmetry parameters, away from their *a*

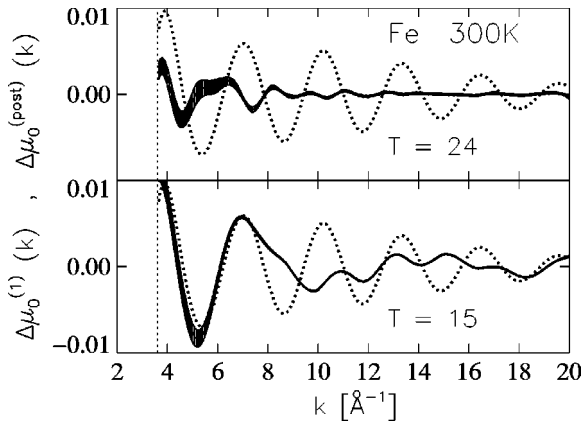

FIG. 8. The dotted line gives the distortion $\delta\mu_0^{(L_3)}$, Eq. (4), the full line with the error band is the result of the fit. The upper frame is calculated for $T=24$, the lower frame for $T=15$.

priori values are shown. The fact that all model parameters, except the $\delta\mu_0(k_t)$, remain essentially unchanged by the fit shows that the distortion of μ_0 is properly "recognized" by the procedure and not compensated by various changes of the other model parameters. This is no longer true for $T=15$, as shown in Fig. 11.

VII. SUMMARY

We have shown that certain deficiencies in the calculation of the embedded-atom strength μ_0 from given model parameters can be compensated empirically in the inverse problem of fitting *K*-edge data. This is also possible in the more demanding case of overlapping contributions of the three *L* edges in lighter elements. An important prerequisite of the proposed procedure is the determination of an empirical efficiency function $A(k)$ from *k*-averaged data and a similarly *k*-averaged theoretical μ_0.

Determining the correction spline $\delta\mu_0$ simultaneously with the standard EXAFS parameters S_0, E_0, R_i, σ_j^2, and $C_{3;i}$

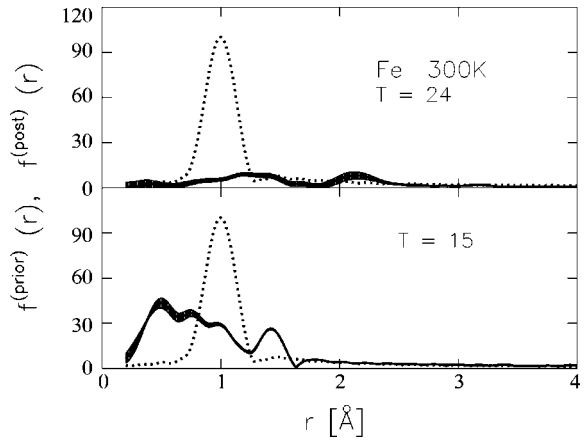

FIG. 9. The functions $f^{(\mathrm{prior})}(r)$ (dotted line) and $f^{(\mathrm{post})}(r)$ (full line) with the error band, in the upper frame for $T=24$, in the lower frame for $T=15$.

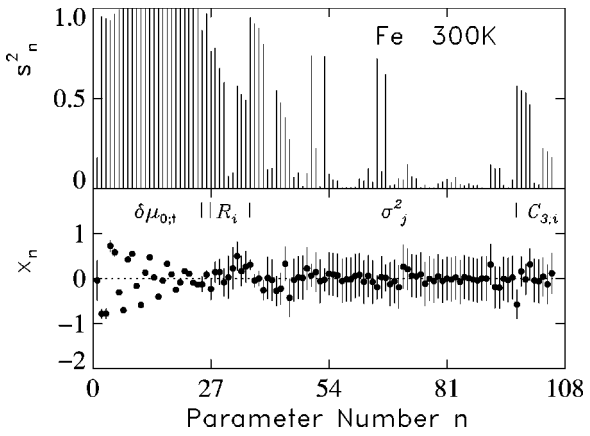

FIG. 10. The same as Fig. 6 for iron *L*-edge data analyzed with a $T=24$ correction spline.

allows us to obtain not only the *a posteriori* errors, but also the cross correlations between all these quantities.

APPENDIX: A SMOOTHING PROCEDURE

In order to obtain a continuous, smoothed, average $\overline{U}(x)$ of a function $U(x_l)$, given at a finite number of discrete points $x_1,\ldots x_L$, Strutinsky and Ivanjuk[16] proposed the following procedure. One generates the orthonormal polynomials $P_k(x)$ on the set of points $x_1,\ldots x_L$ to a weight function $\omega(x)$

$$\sum_{l=1}^{L} P_k(x_l)P_{k'}(x_l)\omega(x_l) = \delta_{kk'}, \quad k,k' < L \tag{A1}$$

by the recursion relations

$$\tilde{P}_{k+1}(x) = (x - b_k)P_k(x) - a_k P_{k-1}(x),$$

$$a_{k+1}^2 = \sum_{l=1}^{L} x_l P_k(x_l)\tilde{P}_{k+1}(x_l)\omega(x_l),$$

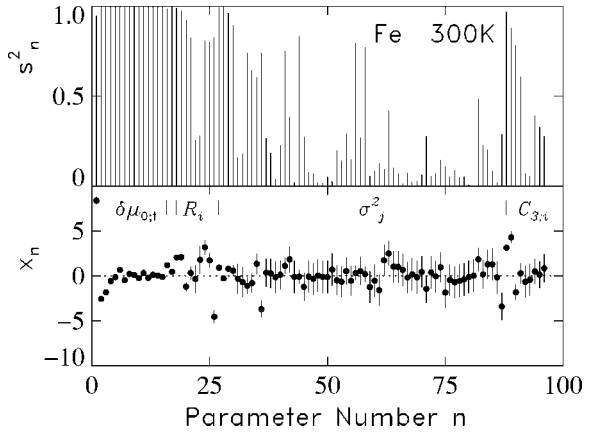

FIG. 11. The same as Fig. 6 for iron *L*-edge data analyzed with a $T=15$ correction spline.

$$P_{k+1}(x) = \frac{1}{a_{k+1}} \tilde{P}_{k+1}(x),$$

$$b_{k+1} = \sum_{l=1}^{L} x_l P_{k+1}^2(x_l) \omega(x_l),$$

valid for $0 \leqslant k < L$ with the initial values

$$P_0(x) = \left(\sum_{l=1}^{L} \omega(x_l) \right)^{-1/2},$$

$$a_0 P_{-1} = 0,$$

$$b_0 = \frac{\sum_l x_l \omega(x_l)}{\sum_l \omega(x_l)}, \tag{A2}$$

and with the convention $a_k > 0$. It is easy to show by induction that the orthonormality relations (A1) follow from the recursion relations. A smoothed function $\overline{U}(x)$ is obtained by expanding $U(x)$ in the set of polynomials $P_k(x)$, retaining only the K lowest terms

$$\overline{U}(x) = \sum_{k=1}^{K} a_k P_k(x),$$

with

$$a_k = \sum_{l=1}^{L} U(x_l) P_k(x_l) \omega(x_l).$$

For the weight function $\omega(x)$, Strutinsky proposed

$$\omega(x) = \left[1 - \left(\frac{x_L - x}{x_L - x_1} \right)^2 \right]^{\alpha}, \quad \alpha > 0.$$

The recursion relations are unstable with the initial conditions (A2). But since we use rather small K values, the loss in numerical accuracy remains tolerable for $k \leqslant K$. In our applications we choose the first support point just below k_{cut}. The exponent α in the weight function and the polynomial order K were obtained from the minimum of the function

$$h(\alpha, K) = \left(\frac{\sum_{l=1}^{L} [U(x_l) - \overline{U}(x_l)]}{\sum_{l=1}^{L} |U(x_l) - \overline{U}(x_l)|} \right)^2.$$

[1] J. J. Rehr, C. H. Booth, F. Bridges, and S. I. Zabinsky, Phys. Rev. B **49**, 12 347 (1994).

[2] L. Campbell, L. Hedin, J. J. Rehr, and W. Bardyszewski, Phys. Rev. B **65**, 064107 (2002).

[3] S. I. Zabinsky, J. J. Rehr, A. Ankudinov, R. Albers, and M. J. Eller, Phys. Rev. B **52**, 2995 (1995); A. L. Ankudinov, Ph.D. thesis, Univ. of Washington (1996).

[4] J. A. Victoreen, J. Appl. Phys. **19**, 855 (1948); *International Tables for X-Ray Crystallography III*, edited by K. Lonsdale *et al.* (Kynoch, Birmingham, England, 1962), Sec. 3.2.

[5] L. A. Bugaev, A. P. Sokolenko, H. V. Dmitrienko, and A. M. Flank, Phys. Rev. B **65** 024105 (2001).

[6] K. V. Klementev, J. Phys. D **34**, 209 (2001).

[7] E. A. Stern, in *X-Ray Absorption*, edited by D. C. Koningsberger and R. Prins (Wiley, New York, 1988), p. 3.

[8] G. Bunker, Nucl. Instrum. Methods Phys. Res. **207**, 437 (1983).

[9] H. J. Krappe and H. H. Rossner, Phys. Rev. B **66**, 184303 (2002).

[10] J. Skilling, in *Maximum Entropy in Action*, edited by B. Buck and V. A. Macaulay (Oxford University, Oxford, 1991), Chap. 2.

[11] V. F. Turchin and V. Z. Nozik, Izv. Akad. Nauk SSSR, Ser. Fiz. Atm. Okeana **5**, 29 (1969) [Bull. Acad. Sci. USSR, Atmos. Oceanic Phys. **5**, 14 (1969)].

[12] M. Newville, Ph.D. thesis, University of Washington, 1994 (private communication).

[13] M. Newville, P. Livins, Y. Yacoby, J. J. Rehr, and E. A. Stern, Phys. Rev. B **47**, 14 126 (1993).

[14] E. A. Stern, M. Newville, B. Ravel, Y. Yacoby, and D. Haskel, Physica B **208&209**, 117 (1995).

[15] R. W. G. Wyckoff, *Crystal Structures* (Wiley, New York, 1963), Vol. 1.

[16] V. M. Strutinsky and F. A. Ivanjuk, Nucl. Phys. A **255**, 405 (1975).